

Imaginary Stark Skin Effect

Heng Lin,¹ Jinghui Pi,^{1,*} Yunyao Qi,¹ and Gui-Lu Long^{1,2,3,4,†}

¹State Key Laboratory of Low-Dimensional Quantum Physics and
Department of Physics, Tsinghua University, Beijing 100084, China

²Beijing Academy of Quantum Information Sciences, Beijing 100193, China

³Frontier Science Center for Quantum Information, Beijing 100084, China

⁴Beijing National Research Center for Information Science and Technology, Beijing 100084, China

The non-Hermitian skin effect (NHSE) is a unique phenomenon in non-Hermitian systems. However, studies on NHSE in systems without translational symmetry remain largely unexplored. Here, we unveil a new class of NHSE, dubbed “imaginary Stark skin effect” (ISSE), in a one-dimensional lossy lattice with a spatially increasing loss rate. The energy spectrum of this model exhibits a T-shaped feature, with approximately half of the eigenstates localized at the left boundary. These skin modes exhibit peculiar behaviors, expressed as a single stable exponential decay wave within the bulk region. We use the transfer matrix method to analyze the formation of the ISSE in this model. According to the eigen-decomposition of the transfer matrix, the wave function is divided into two parts, one of which dominates the behavior of the skin modes in the bulk. Our findings provide insights into the NHSE in systems without translational symmetry and contribute to the understanding of non-Hermitian systems in general.

Introduction. — The study of non-Hermitian quantum physics has gained significant attention in the past two decades due to its unique properties and potential applications in various fields [1–25]. One of the intriguing phenomena is the non-Hermitian skin effect (NHSE), namely the boundary localization of an extensive number of eigenstates [26–28]. The NHSE can lead to novel phenomena absent in its Hermitian counterparts, including unidirectional physical effects [29–31], critical phenomena [32–35], and geometrical related effects in higher dimensions [36–40]. The research on the NHSE has motivated a new theoretical framework for non-Hermitian system, known as non-Bloch band theory [27, 41–43], which establishes the concept of the generalized Brillouin zone (GBZ), providing a powerful tool to understand the NHSE and its topological properties [44–55].

Besides translational symmetric systems, NHSE has also been investigated in systems without translational invariance. However, most of these studies are concentrated on quasicrystals [56–62], systems with disorder [63–70] or impurities [71–74]. In this paper, we unveil a new class of NHSE, termed “imaginary Stark skin effect” (ISSE), in a one-dimensional lossy lattice with a nonuniform loss rate. We focus on the case where the loss rate increases with the lattice index and approaches infinity as the lattice index goes to infinity. This scenario resembles a lattice subjected to a leftward imaginary field, which is the meaning of the term ‘imaginary Stark’ in ISSE. We find that the energy spectrum of this model displays a T-shaped feature [75], with eigenstates from the upper half of the spectrum localized at the left boundary. Surprisingly, these skin modes exhibit an almost uniform decay rate within the bulk region, despite the broken translational invariance. Moreover, numerical results indicate that these skin modes can be approximately expressed as a single exponential decay wave within the bulk region,

which differs from the superposition of two exponential decay waves in conventional NHSE. The broken translational symmetry renders non-Bloch band theory inapplicable for this model. Thus, we analyze these states using the transfer matrix method and reveal the relationship between ISSE and the convergence speed of the transfer matrix eigenvalues. The wave function is divided into two parts based on the eigen-decomposition of the transfer matrix, with one component dominates the behavior of the skin modes in the bulk, thus accounting for the peculiar behavior of ISSE.

Model. — We consider a one-dimensional lossy lattice [Fig. 1]. The eigenequation of this model is

$$\begin{aligned} E\psi_n^A &= t_1\psi_n^B + \frac{t_2}{2}(\psi_{n-1}^B + \psi_{n+1}^B) + i\frac{t_2}{2}(\psi_{n-1}^A - \psi_{n+1}^A), \\ E\psi_n^B &= t_1\psi_n^A + \frac{t_2}{2}(\psi_{n-1}^A + \psi_{n+1}^A) - i\frac{t_2}{2}(\psi_{n-1}^B - \psi_{n+1}^B) \\ &\quad - i\gamma_n\psi_n^B, \end{aligned} \quad (1)$$

where $\psi_n^{A(B)}$ denotes the wave function in sublattices A(B) of unit cell n , L is the chain length, and γ_n represents the loss rate in different B sublattices. When γ_n is uniform, this model can be transformed to the non-

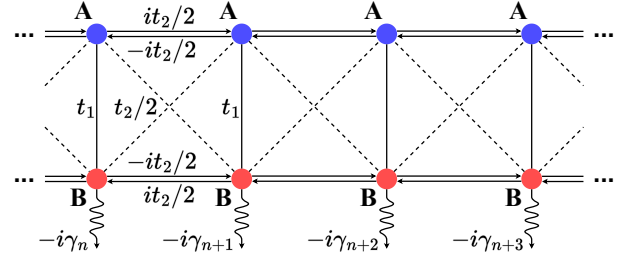


FIG. 1. The one-dimensional non-Hermitian lattices with a nonuniform loss rate γ_n .

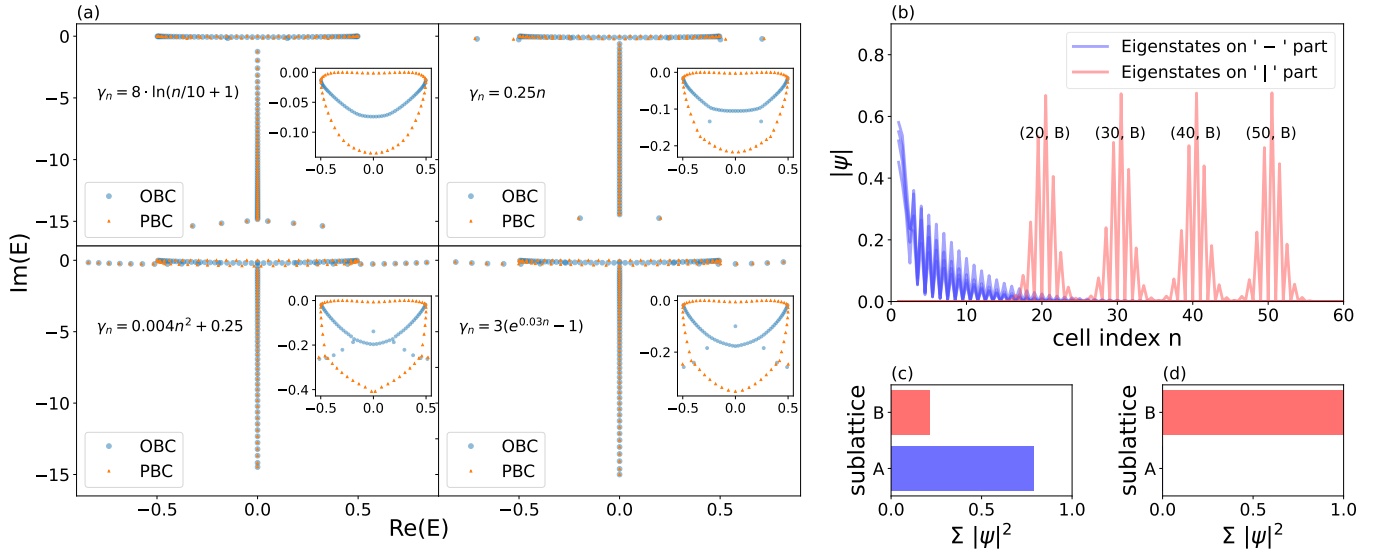


FIG. 2. (a) The energy spectrum for logarithmic, linear, quadratic, and exponential loss rate function γ_n . The insets are the '−' part of spectra (b) The profile of eigenstates from the '−' and '|' parts of T-shaped spectrum. The eigenstates are numbered from large imaginary parts to small imaginary parts. 8 eigenstates are displayed, of which 4 are in the '−' part (eigenstate 20, 30, 40, 50) and the other 4 are in the '|' part (eigenstate 80, 90, 100, 110). The coordinate (n, B) is the position of the peak of the eigenstate in the '|' part. (c), (d) The average probability of particle in sublattice A and B, $\langle \sum_n |\psi_i(n, S)|^2 \rangle_{\psi_i}$, where $S \in \{A, B\}$, and ψ_i denotes wave function of eigenstates in '−' (c) or '|' (d) part of T-shaped spectrum. For (b)-(d), the loss rate $\gamma_n = 0.25n$. For (a)-(d), $t_1 = 0.4$, $t_2 = 0.5$, and the chain length $L = 60$.

Hermitian Su-Schrieffer-Heeger (SSH) model with asymmetric hopping, whose NHSE has been completely studied [27]. In this paper, we focus on the case where γ_n is monotonically increasing with n and satisfies

$$\lim_{n \rightarrow \infty} \gamma_n \rightarrow \infty, \quad (2)$$

and the situation of open boundary condition (OBC) is mainly considered. The energy spectrum of this model exhibit a T-shaped feature, as shown in Fig. 2(a). Furthermore, the eigenstates in the '−' part of T-shaped spectrum exhibit a marked distinction from those in the '|' part. The eigenstates in the '−' part localize at the left boundary, manifesting the NHSE. This is also supported by the observation that the '−' part of periodic boundary condition (PBC) spectra form loops, encircling the '−' part of OBC spectra [42, 76, 77], as in Fig. 2(a) inset. Conversely, the eigenstates in the '|' part are localized around each sublattice B within the bulk region [Fig. 2(b)]. Notably, the eigenstates in the '−' part primarily reside in sublattice A [Fig. 2(c)], whereas those in '|' part predominantly occupy in sublattice B [Fig. 2(d)]. This observation suggests a relative independence between the chains A and B.

To gain insights, we turn off the coupling between sublattices A and B. Then the model becomes two independent chains A and B. We use $E^{(0)}$ and E to represent energy in A-B decoupled and coupled cases, respectively. The energy of chain A is laid on the real axis with $E^{(0)} = t_2 \sin k$, whose eigenstates are extended standing

waves. In the chain B, each site is linked to an eigenstate localized around it, with an energy closely approximated by its imaginary potential, which is similar to the Wannier-Stark localization [78, 79]. The superposition of the spectra of chains A and B results in a T-shaped spectrum, where the energy of chain A forms '−' part and the energy of chain B forms '|' part [Fig. 3(a)]. Upon introducing the coupling between sublattices A and B, the spectrum undergoes certain distortions but retains its overall T-shape [Fig. 3(b)]. For the A-B coupled case, the eigenstates corresponding to the '|' part are still localized around their respective sublattices B. However, the NHSE appears in the eigenstates in '−' part.

ISSE. — For simplicity, we regard each unit cell as a pseudo spin and perform a $\pi/2$ -rotation along the x-axis to each spin. Then the eigenequation becomes a more concise form

$$\begin{aligned} E\psi_n^{A'} &= -i\frac{\gamma_n}{2}\psi_n^{A'} + t_2\psi_{n-1}^{B'} + (t_1 + \frac{\gamma_n}{2})\psi_n^{B'}, \\ E\psi_n^{B'} &= -i\frac{\gamma_n}{2}\psi_n^{B'} + (t_1 - \frac{\gamma_n}{2})\psi_n^{A'} + t_2\psi_{n+1}^{A'}, \end{aligned} \quad (3)$$

where A' and B' are the new Z-basis of pseudo spin after rotation transformation. In the following sections, we will use this basis unless otherwise specified.

The ISSE in this model has two features. First, although the loss rate γ_n is spatially increasing in the lattice, the skin modes have almost uniform decay rate within the bulk region, illustrated by the wave function's linearity on a logarithmic scale [Fig. 4(b)]. Sec-

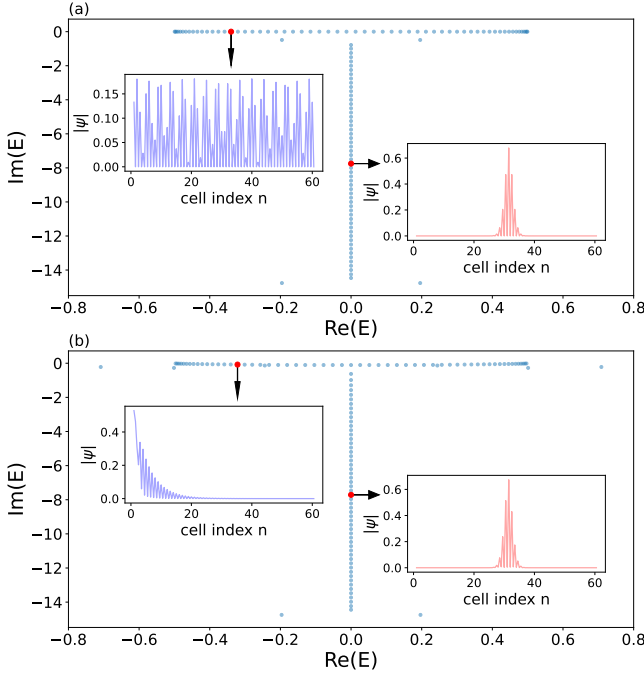


FIG. 3. Energy spectrum for turning off (a) and turning on (b) the coupling between sublattices A and B. The left and right insets are profiles of eigenstate 40 and eigenstate 150. The parameters are $t_1 = 0.4$, $t_2 = 0.5$, $\gamma_n = 0.25n$, and the chain length $L = 60$.

ond, for one-dimensional spatially periodic tight-binding non-Hermitian models, the eigenstates can be written as a superposition of two exponential decay waves [41],

$$\psi_n = (\beta_m)^n \phi^{(m)} + (\beta_{m+1})^n \phi^{(m+1)}, \quad (4)$$

To construct continuum bands under open boundary conditions it requires $|\beta_m| = |\beta_{m+1}|$, so that two decay waves would generate interference fringes and cancel out each other on the boundary [Fig. 4(a)]. However, in our model, numerical results show the absence of interference fringes, indicating that the skin modes can be approximately expressed as a single exponential decay wave within the bulk region [Fig. 4(b)], i.e.

$$\psi_n^{S'} \sim (\beta)^n, \quad (5)$$

where $S' \in \{A', B'\}$ denotes the sublattice, which is very different from that in spatially periodic models.

We first adopt a rough approach to obtain β in Eq. (5). Take the ansatz

$$\psi_n^{S'} = (\beta + \delta_n) \psi_{n-1}^{S'}, \quad (6)$$

where $\delta_n \ll \beta$. Then the bulk eigenequation of Hamiltonian Eq. (3) becomes

$$\begin{aligned} \left(E + i\frac{\gamma_n}{2}\right) \psi_n^{A'} - \left[t_1 + \frac{\gamma_n}{2} + t_2(\beta + \delta_n)^{-1}\right] \psi_n^{B'} &= 0, \\ \left[t_1 - \frac{\gamma_n}{2} + t_2(\beta + \delta_{n+1})\right] \psi_n^{A'} - \left(E + i\frac{\gamma_n}{2}\right) \psi_n^{B'} &= 0, \end{aligned} \quad (7)$$

which leads to

$$0 = \gamma_n \left\{ iE - \frac{t_2}{2} [(\beta + \delta_{n+1}) - (\beta + \delta_n)^{-1}] \right\} + E^2 - [t_1 + t_2(\beta + \delta_n)^{-1}] [t_1 + t_2(\beta + \delta_{n+1})]. \quad (8)$$

To make this equation hold for arbitrary n , the γ_n term $\{iE - \frac{t_2}{2} [(\beta + \delta_{n+1}) - (\beta + \delta_n)^{-1}]\}$ should be approximate to zero, which has two solutions:

$$\beta_{\pm} \approx \frac{iE}{t_2} \left[1 \pm \sqrt{1 - (t_2/E)^2} \right]. \quad (9)$$

The solution β_- is in agreement with the numerical values of β .

Transfer matrix method. — The above approach can not explain why β_- instead of β_+ fits β and how the ISSE arises. In the following part, we analyze the model more accurately via transfer matrix method [80, 81]. Consider the bulk eigen-equation projected on bases $|n-1, B'\rangle$ and $|n, A'\rangle$: $\langle n-1, B'|H'|\psi\rangle = \langle n-1, B'|E|\psi\rangle$ and $\langle n, A'|H'|\psi\rangle = \langle n, A'|E|\psi\rangle$, which can be rewritten in terms of transfer matrix as (see details in [82])

$$|\psi(n)\rangle = T(n) |\psi(n-1)\rangle, \quad (10)$$

where $|\psi(n)\rangle = (\psi_n^{A'}, \psi_n^{B'})^T$, and $T(n)$ is the 2×2 transfer matrix between cell $(n-1)$ and cell n . The transfer matrix describes the relation of eigenstate wave function between two adjacent cells. If γ_n is uniform, $T(n) = T = \sum_i \lambda_i |\lambda_{iR}\rangle \langle \lambda_{iL}|$ is a constant matrix, and $|\psi(n)\rangle = (T)^{n-1} |\psi(1)\rangle = \sum_i \lambda_i^{n-1} \langle \lambda_{iL} | \psi(1) \rangle |\lambda_{iR}\rangle$, which degenerates to the ansatz of non-Bloch band theory, with λ_i corresponding to the β_i . In our model, $T(n)$ is a function of n , with two eigenvalues, whose eigenequation can be written as:

$$\lambda(n)^2 + b(n)\lambda(n) + c(n) = 0, \quad (11)$$

where

$$\begin{aligned} b(n) &= \frac{1}{t_2(t_1 + \gamma_n/2)} \left[t_1^2 + t_2^2 - E^2 + \frac{\gamma_n - \gamma_{n-1}}{2} t_1 \right. \\ &\quad \left. - i \frac{\gamma_n + \gamma_{n-1}}{2} E \right], \\ c(n) &= \frac{t_1 - \gamma_{n-1}/2}{t_1 + \gamma_n/2}, \end{aligned} \quad (12)$$

we denote these two eigenvalues as $\lambda^{(\pm)}(n) = \frac{1}{2} \left(-b(n) \pm \sqrt{b(n)^2 - 4c(n)} \right)$ with left eigenvectors $\langle \lambda_L^{(\pm)}(n) |$ and right eigenvectors $|\lambda_R^{(\pm)}(n)\rangle$, which are orthonormal and complete.

Notice that $b(n)$ and $c(n)$ approach constant value b_0 and c_0 as n approaches infinity:

$$\lim_{n \rightarrow \infty} b(n) \rightarrow b_0 = -2iE/t_2, \quad \lim_{n \rightarrow \infty} c(n) \rightarrow c_0 = -1, \quad (13)$$

then we have

$$\lim_{n \rightarrow \infty} \lambda^{(\pm)}(n) \rightarrow \lambda_0^{(\pm)} = \frac{iE}{t_2} \left[1 \pm \sqrt{1 - (t_2/E)^2} \right], \quad (14)$$

which is the same as β_{\pm} derived from the rough approach in Eq. (9). Recall that the ‘-’ part of T-shaped spectrum is $E_0 = t_2 \sin k$ in the A-B decoupled case. Analogously, here we define $\kappa = \arcsin(E/t_2)$, then Eq. (14) becomes $\lambda_0^{(\pm)} = \pm e^{\pm i\kappa}$ [83], which corresponds to the Bloch phase factor $\pm e^{\pm ik}$ in the A-B decoupled case. It’s easy to verify that $|\lambda_0^{(+)}| > 1$ and $|\lambda_0^{(-)}| < 1$ [82], which is consistent with the numerical results.

Next, we examine the convergence of $\lambda^{(\pm)}(n)$ towards $\lambda_0^{(\pm)}$. As illustrated in Fig. 4(c), $\lambda^{(-)}(n)$ converges notably faster than $\lambda^{(+)}(n)$. Here we give a concise idea of the proof for this observation. For convenience, we assume that γ_n takes the form of linear function $\gamma_n = \gamma_0 n$. A detailed proof for various types of γ_n functions can be found in [82]. To analyze the speed of convergence, we perform Laurent expansion on $b(n)$, $c(n)$ and $\lambda^{(\pm)}(n)$,

$$\begin{aligned} b(n) &= b_0 + b_1/\gamma_n + \dots, \\ c(n) &= c_0 + c_1/\gamma_n + \dots, \\ \lambda^{(\pm)}(n) &= \lambda_0^{(\pm)} + \lambda_1^{(\pm)}/\gamma_n + \dots \end{aligned} \quad (15)$$

Combine Eq. (11), Eq. (12) and Eq. (15), we can derive

$$\frac{\lambda_1^{(\pm)}}{\lambda_0^{(\pm)}} = \mp \frac{(t_1 \pm t_2 \cos \kappa)(t_1 \pm t_2 \cos \kappa + \gamma_0/2)}{t_2 \cos \kappa}, \quad (16)$$

which characterizes the convergence speed of $\lambda^{(\pm)}(n)$ — smaller $\lambda_1^{(\pm)}/\lambda_0^{(\pm)}$ means smaller $1/\gamma_n$ term, and faster convergence. In supplemental material we argue that in the thermodynamic limit the ‘-’ part of spectrum in A-B coupled case will be closed to that in decoupled cases [82], so κ can be closely approximated by k in A-B decoupled case, which ranges from $-\pi/2$ to $\pi/2$. Therefore, from Eq. (16), it follows that $|\lambda_1^{(-)}/\lambda_0^{(-)}| < |\lambda_1^{(+)}/\lambda_0^{(+)}|$. In particular, $|\lambda_1^{(-)}/\lambda_0^{(-)}|$ approaches zero when $\cos \kappa$ is near t_1/t_2 or $(t_1 + \gamma_0/2)/t_2$, which leads to a much faster convergence speed of $\lambda^{(-)}(n)$.

Now we can analyze the formation of the ISSE states in this model. We decompose $|\psi(n)\rangle$ to the eigenvectors of $T(n)$,

$$|\psi(n)\rangle = \psi_n^{(+)} |\lambda_R^{(+)}(n)\rangle + \psi_n^{(-)} |\lambda_R^{(-)}(n)\rangle, \quad (17)$$

where $\psi_n^{(\pm)} = \langle \lambda_L^{(\pm)}(n) | \psi(n) \rangle$, denoting the $\langle \lambda_L^{(\pm)}(n) |$ component of $|\psi(n)\rangle$. If γ_n is uniform, along with Eq. (10), we get the relation between $\psi_{n-1}^{(\pm)}$ and $\psi_n^{(\pm)}$: $\psi_n^{(\pm)} = \lambda^{(\pm)} \psi_{n-1}^{(\pm)}$. This is straightforward—the $\langle \lambda_L^{(\pm)} |$ component, $\psi_n^{(\pm)}$, is scaled by the corresponding eigenvalue $\lambda^{(\pm)}$. Back to the nonuniform γ_n , we can take the approximation that [82]

$$\psi_n^{(\pm)} \approx \lambda^{(\pm)}(n) \psi_{n-1}^{(\pm)}. \quad (18)$$

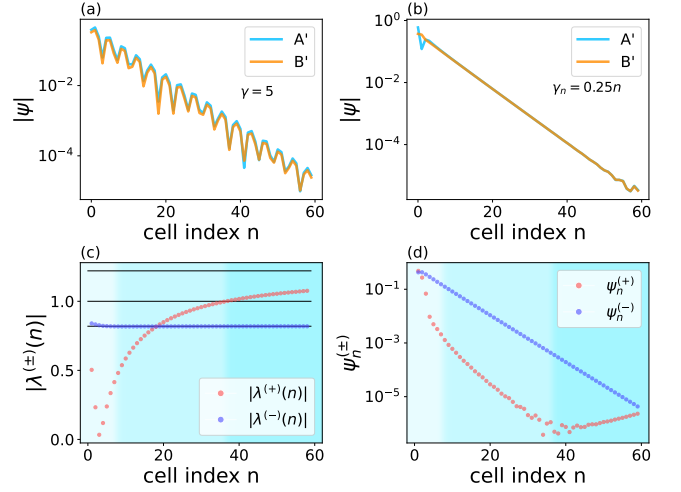


FIG. 4. (a), (b) The profile of eigenstates for uniform loss rate and linear loss rate. For uniform loss rate, two exponential decay waves generate interference fringe in the bulk, while for linear loss rate case, only one exponential decay wave dominates the wave function. (c) The modulus of eigenvalues of transfer matrix $|\lambda^{(\pm)}(n)|$ as a function of n . The three horizontal black lines from top to bottom are $\lambda_0^{(+)}$, 1, $\lambda_0^{(-)}$. (d) The decomposition component of wave function, $\psi_n^{(\pm)}$, varies with n . The parameters are $t_1 = 0.4$, $t_2 = 0.5$, chain length $L = 60$, $\gamma = 5$ for (a) and $\gamma_n = 0.25n$ for (b)-(d).

Fig. 4(d) shows how $\psi_n^{(\pm)}$ evolves with n . The component of $|\psi(n)\rangle$, $\psi_n^{(+)}$ and $\psi_n^{(-)}$, should be in the same order at two edges, so they can cancel out each other to satisfy OBCs $|\psi(0)\rangle = |\psi(L+1)\rangle = 0$. Then we divide the wave function into three stages for different n , as shown in Fig. 4(c) and Fig. 4(d). These three stages can be roughly viewed as the left boundary region, the bulk region, and the right boundary region. In the first stage, near the left boundary, $\psi_n^{(+)}$ and $\psi_n^{(-)}$ begin at the same order. $\lambda^{(-)}(n)$ converges to $\lambda_0^{(-)}$ quickly, so according to Eq. (18), $\psi_n^{(-)}$ acts as an exponential decay wave $\psi_n^{(-)} \sim (\lambda_0^{(-)})^n$. While when γ_n increases from 0 and approaches $2t_1$, $\lambda^{(+)}(n) = c(n)/\lambda^{(-)}(n) \approx (t_1 - \gamma_{n-1}/2) / [(t_1 + \gamma_n/2)\lambda_0^{(-)}]$ would be near 0, hence $|\psi_n^{(+)}|$ would diminish at a significantly faster rate than $|\psi_n^{(-)}|$, eventually attenuating to an extremely low value. In the second stage, in the middle of eigenstate wave function, $|\psi_n^{(+)}|$ is lower several orders than $|\psi_n^{(-)}|$, so $\psi_n^{(-)}$ will dominate the behavior of $|\psi(n)\rangle$ and keep the rigorously exponentially decaying. As n increases, $|\lambda^{(+)}(n)|$ keeps increasing to approach $|\lambda_0^{(+)}|$, and after $|\lambda^{(+)}(n)|$ exceeding 1, we enter the last stage, near the right boundary. In this stage, since $|\lambda^{(+)}(n)| > 1$, $|\psi_n^{(+)}|$ reverses the decline, starts to increase, and finally approaches the order of $|\psi_n^{(-)}|$ at the right boundary to meet the

OBC. Review these three stages, we see that $|\psi_n^{(-)}|$ is much larger than $|\psi_n^{(+)}|$ in the bulk, so the $\psi_n^{(-)}|\lambda_R^{(-)}(n)\rangle$ part dominates the behavior of $|\psi(n)\rangle$, which scales as $(\lambda_0^{(-)})^n$. The influence of $\psi_n^{(+)}|\lambda_R^{(+)}(n)\rangle$ part becomes apparent only near the boundary, causing fluctuations in wave function at these areas [Fig. 4(b)].

Our analysis shows that the formation of the ISSE in this model demands notably fast convergence speed of $\lambda^{(-)}(n)$, which leads to a single stable exponential decay wave predominantly governs the behavior of the skin modes in the bulk. We discuss the impact of parameters in [82]. An extremely small or large t_1 compared with t_2 would result in a sluggish convergence speed of $\lambda^{(-)}(n)$, which would weaken the features of ISSE. This also supports the relationship between the ISSE and the convergence speed of $\lambda^{(-)}(n)$. Furthermore, we demonstrate that it's possible to exhibit the ISSE in a short lattice, which provides the feasibility of future experimental investigation with finite-size systems on this model [82].

Conclusions. — We investigate a non-Hermitian lattice with nonuniform loss rate. In this model, only almost half of eigenstates exhibit the NHSE with intriguing features, which differ from conventional NHSE. Using the transfer matrix method, we show that the convergence speed of the transfer matrix eigenvalues plays a crucial role in the formation of ISSE. We divide the wave function into two parts according to the eigen-decomposition of the transfer matrix. One part is an exponential decay wave that dominates the behavior of the wave function. While the other part is extremely small within the bulk, and only has a significant effect on the boundary. Our work provides a new perspective on the non-Hermitian systems without translational symmetry.

The authors would like to thank Pengyu Wen for helpful discussion. This work is supported by the National Natural Science Foundation of China under Grants No. 11974205, and No. 61727801, and the Key Research and Development Program of Guangdong province (2018B030325002).

* pijh14@gmail.com

† gllong@tsinghua.edu.cn

- [1] N. Hatano and D. R. Nelson, Phys. Rev. Lett. **77**, 570 (1996).
- [2] N. Hatano and D. R. Nelson, Phys. Rev. B **56**, 8651 (1997).
- [3] C. M. Bender and S. Boettcher, Phys. Rev. Lett. **80**, 5243 (1998).
- [4] C. M. Bender, D. C. Brody, and H. F. Jones, Phys. Rev. Lett. **89**, 270401 (2002).
- [5] M. S. Rudner and L. S. Levitov, Phys. Rev. Lett. **102**, 065703 (2009).
- [6] A. Guo, G. J. Salamo, D. Duchesne, R. Morandotti, M. Volatier-Ravat, V. Aimez, G. A. Siviloglou, and D. N.

- Christodoulides, Phys. Rev. Lett. **103**, 093902 (2009).
- [7] J. M. Zeuner, M. C. Rechtsman, Y. Plotnik, Y. Lumer, S. Nolte, M. S. Rudner, M. Segev, and A. Szameit, Phys. Rev. Lett. **115**, 040402 (2015).
- [8] M. Parto, S. Wittek, H. Hodaei, G. Harari, M. A. Bandres, J. Ren, M. C. Rechtsman, M. Segev, D. N. Christodoulides, and M. Khajavikhan, Phys. Rev. Lett. **120**, 113901 (2018).
- [9] C. M. Bender, Rep. Prog. Phys. **70**, 947 (2007).
- [10] I. Rotter, J. Phys. A **42**, 153001 (2009).
- [11] A. Regensburger, C. Bersch, M.-A. Miri, G. Onishchukov, D. N. Christodoulides, and U. Peschel, Nature **488**, 167 (2012).
- [12] B. Zhen, C. W. Hsu, Y. Igarashi, L. Lu, I. Kaminer, A. Pick, S.-L. Chua, J. D. Joannopoulos, and M. Soljačić, Nature **525**, 354 (2015).
- [13] W. Chen, Ş. Kaya Özdemir, G. Zhao, J. Wiersig, and L. Yang, Nature **548**, 192 (2017).
- [14] H. Hodaei, A. U. Hassan, S. Wittek, H. Garcia-Gracia, R. El-Ganainy, D. N. Christodoulides, and M. Khajavikhan, Nature **548**, 187 (2017).
- [15] L. Feng, Y.-L. Xu, W. S. Fegadolli, M.-H. Lu, J. E. B. Oliveira, V. R. Almeida, Y.-F. Chen, and A. Scherer, Nat. Mater. **12**, 108 (2012).
- [16] P. St-Jean, V. Goblot, E. Galopin, A. Lemaître, T. Ozawa, L. Le Gratiet, I. Sagnes, J. Bloch, and A. Amo, Nat. Photonics **11**, 651 (2017).
- [17] R. El-Ganainy, K. G. Makris, M. Khajavikhan, Z. H. Musslimani, S. Rotter, and D. N. Christodoulides, Nat. Phys. **14**, 11 (2018).
- [18] L. Xiao, T. Deng, K. Wang, G. Zhu, Z. Wang, W. Yi, and P. Xue, Nat. Phys. **16**, 761 (2020).
- [19] C. E. Rüter, K. G. Makris, R. El-Ganainy, D. N. Christodoulides, M. Segev, and D. Kip, Nat. Phys. **6**, 192 (2010).
- [20] L. Xiao, X. Zhan, Z. H. Bian, K. K. Wang, X. Zhang, X. P. Wang, J. Li, K. Mochizuki, D. Kim, N. Kawakami, W. Yi, H. Obuse, B. C. Sanders, and P. Xue, Nat. Phys. **13**, 1117 (2017).
- [21] C. Poli, M. Bellec, U. Kuhl, F. Mortessagne, and H. Schomerus, Nat. Commun. **6**, 6710 (2015).
- [22] L. Feng, M. Ayache, J. Huang, Y.-L. Xu, M.-H. Lu, Y.-F. Chen, Y. Fainman, and A. Scherer, Science **333**, 729 (2011).
- [23] B. Bahari, A. Ndao, F. Vallini, A. El Amili, Y. Fainman, and B. Kanté, Science **358**, 636 (2017).
- [24] G. Harari, M. A. Bandres, Y. Lumer, M. C. Rechtsman, Y. D. Chong, M. Khajavikhan, D. N. Christodoulides, and M. Segev, Science **359**, eaar4003 (2018).
- [25] M. A. Bandres, S. Wittek, G. Harari, M. Parto, J. Ren, M. Segev, D. N. Christodoulides, and M. Khajavikhan, Science **359**, eaar4005 (2018).
- [26] V. M. Martinez Alvarez, J. E. Barrios Vargas, and L. E. F. Foa Torres, Phys. Rev. B **97**, 121401(R) (2018).
- [27] S. Yao and Z. Wang, Phys. Rev. Lett. **121**, 086803 (2018).
- [28] S. Yao, F. Song, and Z. Wang, Phys. Rev. Lett. **121**, 136802 (2018).
- [29] F. Song, S. Yao, and Z. Wang, Phys. Rev. Lett. **123**, 170401 (2019).
- [30] C. C. Wanjura, M. Brunelli, and A. Nunnenkamp, Nat. Commun. **11**, 3149 (2020).
- [31] W.-T. Xue, Y.-M. Hu, F. Song, and Z. Wang, Phys. Rev. Lett. **128**, 120401 (2022).

- [32] L. Li, C. H. Lee, S. Mu, and J. Gong, Nat. Commun. **11**, 1 (2020).
- [33] C.-H. Liu, K. Zhang, Z. Yang, and S. Chen, Phys. Rev. Research **2**, 043167 (2020).
- [34] K. Yokomizo and S. Murakami, Phys. Rev. B **104**, 165117 (2021).
- [35] C.-X. Guo, C.-H. Liu, X.-M. Zhao, Y. Liu, and S. Chen, Phys. Rev. Lett. **127**, 116801 (2021).
- [36] X.-Q. Sun, P. Zhu, and T. L. Hughes, Phys. Rev. Lett. **127**, 066401 (2021).
- [37] K. Zhang, Z. Yang, and C. Fang, Nat. Commun. **13**, 1 (2022).
- [38] Y. Li, C. Liang, C. Wang, C. Lu, and Y.-C. Liu, Phys. Rev. Lett. **128**, 223903 (2022).
- [39] W. Zhu and J. Gong, Phys. Rev. B **106**, 035425 (2022).
- [40] C. Wu, A. Fan, and S.-D. Liang, AAPPS Bulletin **32**, 39 (2022).
- [41] K. Yokomizo and S. Murakami, Phys. Rev. Lett. **123**, 066404 (2019).
- [42] K. Zhang, Z. Yang, and C. Fang, Phys. Rev. Lett. **125**, 126402 (2020).
- [43] H.-Y. Wang, F. Song, and Z. Wang, Phys. Rev. X **14**, 021011 (2024).
- [44] D. Leykam, K. Y. Bliokh, C. Huang, Y. D. Chong, and F. Nori, Phys. Rev. Lett. **118**, 040401 (2017).
- [45] H. Shen, B. Zhen, and L. Fu, Phys. Rev. Lett. **120**, 146402 (2018).
- [46] Z. Gong, Y. Ashida, K. Kawabata, K. Takasan, S. Higashikawa, and M. Ueda, Phys. Rev. X **8**, 031079 (2018).
- [47] K. Kawabata, S. Higashikawa, Z. Gong, Y. Ashida, and M. Ueda, Nat. Commun. **10**, 297 (2019).
- [48] K. Kawabata, K. Shiozaki, M. Ueda, and M. Sato, Phys. Rev. X **9**, 041015 (2019).
- [49] H. Zhou and J. Y. Lee, Phys. Rev. B **99**, 235112 (2019).
- [50] D. S. Borgnia, A. J. Kruchkov, and R.-J. Slager, Phys. Rev. Lett. **124**, 056802 (2020).
- [51] K. Kawabata, T. Bessho, and M. Sato, Phys. Rev. Lett. **123**, 066405 (2019).
- [52] Y. Xiong, J. Phys. Commun. **2**, 035043 (2018).
- [53] C. H. Lee and R. Thomale, Phys. Rev. B **99**, 201103(R) (2019).
- [54] T. Liu, Y.-R. Zhang, Q. Ai, Z. Gong, K. Kawabata, M. Ueda, and F. Nori, Phys. Rev. Lett. **122**, 076801 (2019).
- [55] C. H. Lee, L. Li, and J. Gong, Phys. Rev. Lett. **123**, 016805 (2019).
- [56] H. Jiang, L.-J. Lang, C. Yang, S.-L. Zhu, and S. Chen, Phys. Rev. B **100**, 054301 (2019).
- [57] X. Cai, Phys. Rev. B **103**, 014201 (2021).
- [58] Y. Liu, Y. Wang, X.-J. Liu, Q. Zhou, and S. Chen, Phys. Rev. B **103**, 014203 (2021).
- [59] C. Yuce and H. Ramezani, Phys. Rev. B **106**, 024202 (2022).
- [60] S. Manna and B. Roy, Commun. Phys. **6**, 10 (2023).
- [61] A. Chakrabarty and S. Datta, Phys. Rev. B **107**, 064305 (2023).
- [62] L. Zhou, Phys. Rev. B **108**, 014202 (2023).
- [63] S. Longhi, Opt. Lett. **45**, 5250 (2020).
- [64] J. Claes and T. L. Hughes, Phys. Rev. B **103**, L140201 (2021).
- [65] S. Longhi, Phys. Rev. B **103**, 144202 (2021).
- [66] K.-M. Kim and M. J. Park, Phys. Rev. B **104**, L121101 (2021).
- [67] B. A. Bhargava, I. C. Fulga, J. van den Brink, and A. G. Moghaddam, Phys. Rev. B **104**, L241402 (2021).
- [68] R. Sarkar, S. S. Hegde, and A. Narayan, Phys. Rev. B **106**, 014207 (2022).
- [69] K. Suthar, Y.-C. Wang, Y.-P. Huang, H. H. Jen, and J.-S. You, Phys. Rev. B **106**, 064208 (2022).
- [70] H. Liu, M. Lu, Z.-Q. Zhang, and H. Jiang, Phys. Rev. B **107**, 144204 (2023).
- [71] L. Li, C. H. Lee, and J. Gong, Commun. Phys. **4**, 42 (2021).
- [72] F. Roccati, Phys. Rev. A **104**, 022215 (2021).
- [73] C.-X. Guo, C.-H. Liu, X.-M. Zhao, Y. Liu, and S. Chen, Phys. Rev. Lett. **127**, 116801 (2021).
- [74] P. Mognini, O. Arandes, and E. J. Bergholtz, Phys. Rev. Res. **5**, 033058 (2023).
- [75] C. Yuce and H. Ramezani, Phys. Rev. B **107**, L140302 (2023).
- [76] N. Okuma, K. Kawabata, K. Shiozaki, and M. Sato, Phys. Rev. Lett. **124**, 086801 (2020).
- [77] K. Zhang, Z. Yang, and C. Fang, Nat. Commun. **13**, 2496 (2022).
- [78] G. H. Wannier, Rev. Mod. Phys. **34**, 645 (1962).
- [79] T. Hartmann, F. Keck, H. Korsch, and S. Mossmann, New J. Phys. **6**, 2 (2004).
- [80] M. Kohmoto, B. Sutherland, and C. Tang, Phys. Rev. B **35**, 1020 (1987).
- [81] F. K. Kunst and V. Dwivedi, Phys. Rev. B **99**, 245116 (2019).
- [82] See Supplemental Material at [URL_will_be_inserted_by_publisher](#) for the details.
- [83] Here we choose the principal branch of square root function in Eq. (14) to make it single-valued, by defining the angle of the argument of square root to be in $[0, 2\pi)$.

Supplemental Material for “Imaginary Stark Skin Effect”

Heng Lin,¹ Jinghui Pi,^{1,*} Yunyao Qi,¹ and Gui-Lu Long^{1,2,3,4,†}

¹*State Key Laboratory of Low-Dimensional Quantum Physics and
Department of Physics, Tsinghua University, Beijing 100084, China*

²*Beijing Academy of Quantum Information Sciences, Beijing 100193, China*

³*Frontier Science Center for Quantum Information, Beijing 100084, China*

⁴*Beijing National Research Center for Information Science and Technology, Beijing 100084, China*

CONTENTS

I. Derivation of transfer matrix	1
II. The modulus of $\lambda_0^{(\pm)}$	2
III. Energy change between A-B decoupled and coupled systems	2
IV. Convergence property of transfer matrix eigenvalues $\lambda^{(\pm)}(n)$	4
V. The recurrence relation of $\psi_n^{(\pm)}$ and its approximation	6
VI. Analysis of Parameters	7
A. t_1 and t_2	8
B. Chain Length L	8
References	9

I. DERIVATION OF TRANSFER MATRIX

In this section, we give a detailed derivation of transfer matrix. Consider the bulk eigen-equation projected on basis $|n-1, B'\rangle$ and $|n, A'\rangle$: $\langle n-1, B'| H' |\psi\rangle = \langle n-1, B'| E |\psi\rangle$ and $\langle n, A'| H' |\psi\rangle = \langle n, A'| E |\psi\rangle$,

$$\begin{pmatrix} t_1 - \frac{\gamma_{n-1}}{2} & -i\frac{\gamma_{n-1}}{2} - E & t_2 & 0 \\ 0 & t_2 & -i\frac{\gamma_n}{2} - E & t_1 + \frac{\gamma_n}{2} \end{pmatrix} \begin{pmatrix} \psi_{n-1}^{A'} \\ \psi_{n-1}^{B'} \\ \psi_n^{A'} \\ \psi_n^{B'} \end{pmatrix} = 0, \quad (1)$$

which can be rewritten as

$$\begin{pmatrix} t_2 & 0 \\ -i\frac{\gamma_n}{2} - E & t_1 + \frac{\gamma_n}{2} \end{pmatrix} \begin{pmatrix} \psi_n^{A'} \\ \psi_n^{B'} \end{pmatrix} = - \begin{pmatrix} t_1 - \frac{\gamma_{n-1}}{2} & -i\frac{\gamma_{n-1}}{2} - E \\ 0 & t_2 \end{pmatrix} \begin{pmatrix} \psi_{n-1}^{A'} \\ \psi_{n-1}^{B'} \end{pmatrix}. \quad (2)$$

This directly leads to

$$|\psi(n)\rangle = T(n) |\psi(n-1)\rangle, \quad (3)$$

where $|\psi(n)\rangle = (\psi_n^{A'}, \psi_n^{B'})^T$, and $T(n)$ is the transfer matrix between cell $n-1$ and cell n , given by

$$T(n) = - \begin{pmatrix} t_2 & 0 \\ -i\frac{\gamma_n}{2} - E & t_1 + \frac{\gamma_n}{2} \end{pmatrix}^{-1} \begin{pmatrix} t_1 - \frac{\gamma_{n-1}}{2} & -i\frac{\gamma_{n-1}}{2} - E \\ 0 & t_2 \end{pmatrix} = \begin{pmatrix} -\frac{t_1 - \frac{\gamma_{n-1}}{2}}{(E + i\frac{\gamma_n}{2})(t_1 - \frac{\gamma_{n-1}}{2}) - t_2^2} & \frac{E + i\frac{\gamma_{n-1}}{2}}{t_2(t_1 + \frac{\gamma_n}{2})} \\ -\frac{t_2}{t_2(t_1 + \frac{\gamma_n}{2})} & \frac{t_2}{t_2(t_1 + \frac{\gamma_n}{2})} \end{pmatrix}. \quad (4)$$

* pijh14@gmail.com

† gllong@tsinghua.edu.cn

II. THE MODULUS OF $\lambda_0^{(\pm)}$

Let's begin with the conclusion from the main article,

$$\lambda_0^{(\pm)} = \pm e^{\pm i\kappa}, \quad (5)$$

where $\kappa = \arcsin(E/t_2)$. Considering that our system is dissipative, the imaginary part of the eigen-energy must be negative, i.e. $\text{Im}(E) \leq 0$. So $\text{Im}(\kappa)$ would also be negative. Thus, we have:

$$|\lambda_0^{(+)}| = e^{-\text{Im}(\kappa)} > 1, \quad |\lambda_0^{(-)}| = e^{\text{Im}(\kappa)} < 1. \quad (6)$$

III. ENERGY CHANGE BETWEEN A-B DECOUPLED AND COUPLED SYSTEMS

In this section, we show that the energy difference of the ‘-’ part in T-shaped spectrum between the A-B decoupled and A-B coupled lattices vanishes in thermodynamic limit. We denote the A-B decoupled Hamiltonian as $H^{(0)}$ and the A-B coupled Hamiltonian as H . The difference between these Hamiltonians, H' , is defined as $H' := H - H^{(0)}$. The right eigenstates of $H^{(0)}$ are denoted by $|R_i^{(0)}\rangle$ with eigenenergies $E_i^{(0)}$. Furthermore, $E_i^{(0)(-)}$ ($E_i^{(0)(l)}$) and $|R_i^{(0)(-)}\rangle$ ($|R_i^{(0)(l)}\rangle$) denote the eigenenergies and eigenstates belonging to the ‘-’ (‘|’) subspace of the $H^{(0)}$ spectrum, respectively. We use the similar notation E_i , $E_i^{(-)}$ and $E_i^{(l)}$ denote the energy spectrum of the A-B coupled Hamiltonian H .

In the A-B decoupled system, for the ‘-’ part of the spectrum, the eigenenergies are given by $E_i^{(0)(-)} = t_2 \sin k$, where $k = \left(\frac{n}{L+1} - \frac{1}{2}\right)\pi$ and $n = 1, 2, \dots, L$. The corresponding eigenstates are extended standing waves in the bulk, given by: $|R_i^{(0)(-)}\rangle = \sqrt{\frac{2}{L}} \sum_{n=1}^L i^n \sin[(\frac{\pi}{2} - k)n] |n, A\rangle$. For the ‘|’ part of the spectrum, eigenstates are localized around each B site with energy approximately equal to $-i\gamma_n$.

Now we focus on the energy change in the ‘-’ part between A-B decoupled and coupled systems with the following assumption:

Assumption 1 Define $H(t) := H^{(0)} + tH'$ with $t \in [0, 1]$, so that $H(0) = H^{(0)}$ and $H(1) = H$. Consider an eigenvalue in the ‘-’ part of the spectrum of $H^{(0)}$, e.g. $E_i^{(0)(-)}$, and the corresponding eigenvalue in the ‘-’ part of the spectrum of H is $E_i^{(-)}$. Varying the parameter t induces a trajectory of an eigenvalue of $H(t)$, denoted by $E_i(t)$. This trajectory connects $E_i^{(0)}$ and E_i , meaning that $E_i(0) = E_i^{(0)(-)}$ and $E_i(1) = E_i^{(-)}$, without any level crossings.

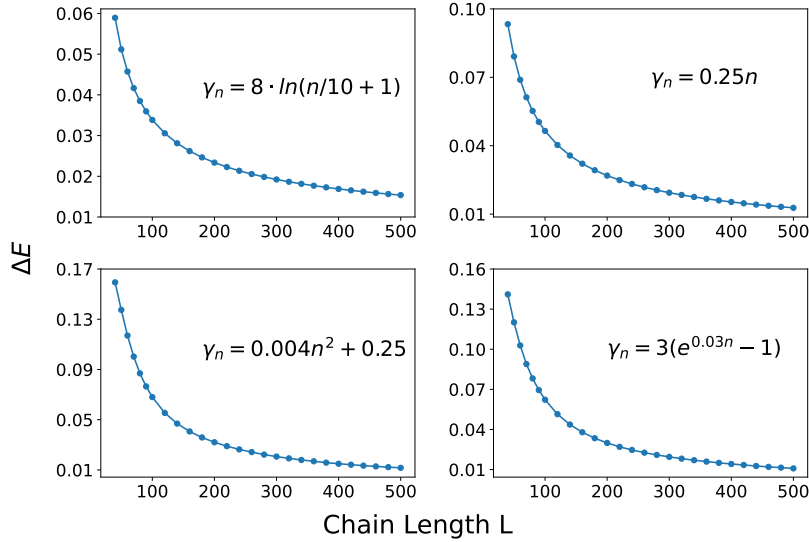


FIG. 1. The average energy difference in ‘-’ part between A-B decoupled and coupled cases, $\Delta E = \frac{1}{N^{(0)(-)}} \sum_i |E_i^{(0)(-)} - E_i^{(-)}|$, where $N^{(0)(-)} = \left| \left\{ E_i^{(0)(-)} \right\}_i \right|$ denotes the number of eigenenergies in the ‘-’ part of the spectrum, as a function of chain length L , for logarithmic, linear, quadratic, and exponential loss rate function. The parameters are $t_1 = 0.4$ and $t_2 = 0.5$.

This assumption is akin to the adiabatic assumption in Hermitian systems. Based on the assumption, we argue that the energy from ‘-’ part in A-B decoupled case converges to that in the coupled cases, namely $E_i^{(0)(-)} \sim E_i^{(-)}$, in the thermodynamic limit.

In Fig. 1, we observe that the average energy difference $\Delta E = \overline{|E_i^{(0)(-)} - E_i^{(-)}|}$ decreases with increasing chain length L . The decrease in ΔE can be attributed to two primary factors. Firstly, with the increase in L , the average separation between energies from ‘-’ part and ‘|’ part increases, scaling as γ_n . Secondly, consider the strength of coupling between $|R_i^{(0)(-)}\rangle$ and eigenstates from ‘|’ part introduced by H' . The eigenstates from ‘|’ part are localized states, and H' is a local coupling. Due to the localized nature, through H' , eigenstates from ‘|’ part can only couple with the part of a wave function that is near them. However, $|R_i^{(0)(-)}\rangle$ is an extended standing wave with an amplitude that diminishes with L , scaling as $\sqrt{1/L}$. Therefore the coupling between $|R_i^{(0)(-)}\rangle$ and eigenstates from ‘|’ part weakens as L increases. These two factors collectively contribute to the attenuation of the virtual process between eigenstates from ‘-’ part and ‘|’ part, leading to a diminishing energy perturbation.

To elaborate further, we can use eigenvalue perturbation to analyze this model, considering H' as the perturbation acting on $H^{(0)}$ [1]. Since H' only couples adjacent A and B sites, the first order perturbation of $E_i^{(0)(-)}$ is zero, and the largest perturbation term comes from the second-order process between $E_i^{(0)(-)}$ and eigenstates in the ‘|’ part, represented by

$$E_i^{(2)(-)} = \sum_j \frac{\langle L_i^{(0)(-)} | H' | R_j^{(0)(l)} \rangle \langle L_j^{(0)(l)} | H' | R_i^{(0)(-)} \rangle}{E_i^{(0)(-)} - E_j^{(0)(l)}}, \quad (7)$$

where $\langle L_i^{(0)(-)} |$ ($\langle L_j^{(0)(l)} |$) are the left eigenstates corresponding to $E_i^{(0)(-)}$ ($E_j^{(0)(l)}$). In the $\langle L_i^{(0)(-)} | H' | R_j^{(0)(l)} \rangle$ term of Eq. (7), $|R_j^{(0)(l)}\rangle$ is a localized wavefunction with a width of $w(j) \sim 1/\gamma_j'$, which is similar to the Wannier-Stark localization [2, 3]. Since H' only couples adjacent A and B sites, $H' |R_j^{(0)(l)}\rangle$ is also a localized wavefunction with a width approximately equal to $w(j)$, and its norm satisfies

$$|H' |R_j^{(0)(l)}\rangle| \leq (t_1 + t_2) |R_j^{(0)(l)}\rangle| = t_1 + t_2, \quad (8)$$

where $t_1 + t_2$ is the largest eigenvalue of H' . However, $\langle L_i^{(0)(-)} | = \sqrt{\frac{2}{L}} \sum_{n=1}^L (-i)^n \sin[(\frac{\pi}{2} - k)n] \langle n, A |$ represents a standing wave extended in the bulk. Consequently, the matrix element $\langle L_i^{(0)(-)} | H' | R_j^{(0)(l)} \rangle$ is bounded by

$$|\langle L_i^{(0)(-)} | H' | R_j^{(0)(l)} \rangle| \leq (t_1 + t_2) \sqrt{\frac{2}{L}} w(j) \sim \frac{1}{\gamma_j' \sqrt{L}}. \quad (9)$$

For $E_i^{(0)(-)} - E_j^{(0)(l)}$ term in Eq. (7), since $|E_j^{(0)(l)}| \gg |E_i^{(0)(-)}|$, we have

$$|E_i^{(0)(-)} - E_j^{(0)(l)}| \geq |E_j^{(0)(l)}| - |E_i^{(0)(-)}| \geq \gamma_j - t_2 - t_2 = \gamma_j - 2t_2. \quad (10)$$

By combining inequalities (9) and (10), the upper bound of $E_i^{(2)(-)}$ can be expressed as

$$E_i^{(2)(-)} \leq \frac{C}{L} \sum_j \frac{1}{\gamma_j'^2 (\gamma_j - 2t_2)} \sim \frac{1}{L} \sum_j \frac{1}{\gamma_j'^2 \gamma_j}, \quad (11)$$

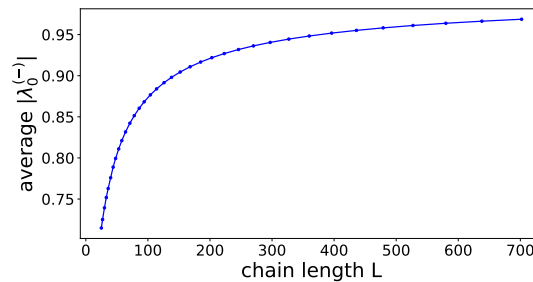


FIG. 2. The average of $|\lambda_0^{(-)}|$ over eigenstates in ‘-’ part of spectrum as a function of chain length L . Average $|\lambda_0^{(-)}|$ increases monotonically and tends to approach 1 as L increases. The parameters are $t_1 = 0.4$, $t_2 = 0.5$ and $\gamma_n = 0.25n$.

where C is a relevant constant. For the polynomial loss rate $\gamma_n = n^\alpha$ with $\alpha \geq 1$ or exponential loss rate, we have

$$\lim_{L \rightarrow \infty} \frac{1}{L} \sum_j \frac{1}{\gamma_j'^2 \gamma_j} = 0, \quad (12)$$

which implies the second order perturbation of energy $E_i^{(2)(-)}$ converges to zero in the thermodynamic limit. Although this upper bound is divergent for logarithmic loss rate, the numerical results suggest that for logarithmic loss rate function, the average energy difference in ‘-’ part between A-B decoupled and coupled cases also decreases as the chain length L increases [Fig. 1].

One might raise the question of why a NHSE state and an extended state share similar energy value. In fact, as the parameter L increases, the NHSE weakens, and the decay rate $\lambda_0^{(-)}$ of the wave function experiences an augmentation toward 1, as illustrated in Fig. 2, which makes the wave function more akin to an extended state. This phenomenon aligns with physical intuition, considering that a larger lattice implies a greater average loss rate in this model, and a lattice with a uniform loss rate will exhibit a weaker NHSE when the loss rate is larger.

IV. CONVERGENCE PROPERTY OF TRANSFER MATRIX EIGENVALUES $\lambda^{(\pm)}(n)$

In the main article, we have stated that $\lambda^{(-)}(n)$ converges much faster than $\lambda^{(+)}(n)$. In this section, we delve into the convergence properties of $\lambda^{(\pm)}(n)$ in detail and establishes the validity of this assertion across a broad range of types of γ_n function.

We start from the eigenequation of transfer matrices $T(n)$, given by

$$\lambda(n)^2 + b(n)\lambda(n) + c(n) = 0, \quad (13)$$

where the expressions of $b(n)$ and $c(n)$ are

$$\begin{aligned} b(n) &= \frac{1}{t_2(t_1 + \gamma_n/2)} \left[t_1^2 + t_2^2 - E^2 + \frac{\gamma_n - \gamma_{n-1}}{2} t_1 - i \frac{\gamma_n + \gamma_{n-1}}{2} E \right], \\ c(n) &= \frac{t_1 - \gamma_{n-1}/2}{t_1 + \gamma_n/2}. \end{aligned} \quad (14)$$

The solutions of Eq. (13) can be expressed as

$$\lambda^{(\pm)}(n) = \frac{1}{2} \left(-b(n) \pm \sqrt{b(n)^2 - 4c(n)} \right). \quad (15)$$

To ensure the single-valuedness of Eq. (15), we employ the principal branch of the square root function, restricting the angle of the square root’s argument to the interval $[0, 2\pi)$.

According to Eq. (14), $b(n)$ and $c(n)$ converge to constant value b_0 and c_0 , respectively, as n approaches infinity. For example, we have

$$\lim_{n \rightarrow \infty} b(n) \rightarrow b_0 = -2iE/t_2, \quad \lim_{n \rightarrow \infty} c(n) \rightarrow c_0 = -1, \quad (16)$$

for the polynomial loss rate $\gamma_n = n^\alpha$, and then $\lambda^{(\pm)}(n)$ converge to

$$\lim_{n \rightarrow \infty} \lambda^{(\pm)}(n) \rightarrow \lambda_0^{(\pm)} = \frac{1}{2} \left(-b_0 \pm \sqrt{b_0^2 - 4c_0} \right) = \frac{iE}{t_2} \left[1 \pm \sqrt{1 - (t_2/E)^2} \right]. \quad (17)$$

To analyze the convergence property of $\lambda^{(\pm)}(n)$, we expand Eq. (14) in terms of $\frac{1}{\gamma_n}$ and obtain,

$$\begin{aligned} b(n) &= b_0 + \frac{\gamma_n - \gamma_{n-1}}{\gamma_n} \frac{t_1 + iE}{t_2} + \frac{1}{\gamma_n} \frac{2(t_1^2 + t_2^2 - E^2 + 2iEt_1)}{t_2} + \frac{b_2}{\gamma_n^2} + \dots, \\ c(n) &= c_0 + \frac{\gamma_n - \gamma_{n-1}}{\gamma_n} + \frac{4t_1}{\gamma_n} + \frac{c_2}{\gamma_n^2} + \dots, \end{aligned} \quad (18)$$

where b_2 and c_2 are the coefficient of $(1/\gamma_n)^2$ term. To isolate the leading-order contribution, we neglect higher-order terms $(1/\gamma_n)^m$ for $m > 1$, keeping only the $\frac{1}{\gamma_n}$ and $\frac{\gamma_n - \gamma_{n-1}}{\gamma_n}$ terms. The form of γ_n determines which one is the leading nontrivial term. Specifically, several different types of γ_n function will be discussed in the following.

(1.) $\lim_{n \rightarrow \infty} (\gamma_n - \gamma_{n-1}) = 0$. For example, logarithmic function $\gamma_n \sim \log n$, or polynomial function with degree smaller than 1, i.e. $\gamma_n \sim n^\alpha$, where $\alpha < 1$.

Apparently, the leading nontrivial term is $1/\gamma_n$ term in this type of γ_n function. Taking the first-order approximation of Eq. (18), we obtain

$$\begin{aligned} b(n) &= b_0 + \frac{b_1}{\gamma_n} + \dots \quad \text{where } b_1 = \frac{2(t_1^2 + t_2^2 - E^2 + 2iEt_1)}{t_2}, \\ c(n) &= c_0 + \frac{c_1}{\gamma_n} + \dots \quad \text{where } c_1 = 4t_1. \end{aligned} \quad (19)$$

Similarly, the expansion of $\lambda^{(\pm)}(n)$ is

$$\lambda^{(\pm)}(n) = \lambda_0^{(\pm)} + \frac{\lambda_1^{(\pm)}}{\gamma_n} + \dots, \quad (20)$$

where $\lambda_1^{(\pm)}$ is the expansion coefficient of $1/\gamma_n$ term. By substituting Eq. (19) and Eq. (20) into Eq. (13), we solve out $\lambda_1^{(\pm)}/\lambda_0^{(\pm)}$, and the result is

$$\frac{\lambda_1^{(\pm)}}{\lambda_0^{(\pm)}} = -\frac{b_1 + c_1/\lambda_0^{(\pm)}}{2\lambda_0^{(\pm)} + b_0}. \quad (21)$$

The quantities $\lambda_1^{(\pm)}/\lambda_0^{(\pm)}$ characterize the convergence speed of $\lambda^{(\pm)}(n)$, e.g. smaller $\lambda_1^{(\pm)}/\lambda_0^{(\pm)}$ means smaller $1/\gamma_n$ term and faster convergence to $\lambda_0^{(\pm)}$.

In the A-B decoupled case, the ‘-’ part of T-shaped spectrum is characterized by $E_0 = t_2 \sin k$, where $k = \left(\frac{n}{L+1} - \frac{1}{2}\right)\pi$ and n ranges from 1 to L . Analogously, we define $\kappa = \arcsin(E/t_2)$, then Eq. (17) becomes

$$\lambda_0^{(\pm)} = \pm e^{\pm i\kappa}, \quad (22)$$

which corresponds to the Bloch phase factor $\pm e^{\pm i\kappa}$. Substituting Eq. (19) and Eq. (22) into Eq. (21), we get

$$\frac{\lambda_1^{(\pm)}}{\lambda_0^{(\pm)}} = \mp \frac{(t_1 \pm t_2 \cos \kappa)^2}{t_2 \cos \kappa}. \quad (23)$$

In Section. III of supplemental material, we argue that in the thermodynamic limit, the ‘-’ part of spectrum in A-B coupled case converges towards that of the decoupled cases. Consequently, the parameter κ in Eq. (23) can be closely approximated by k in A-B decoupled case, which spans the range from $-\pi/2$ to $\pi/2$. We plot $|\lambda_1^{(\pm)}/\lambda_0^{(\pm)}|$ as a function of κ in Fig. 3 (a), which shows $|\lambda_1^{(-)}/\lambda_0^{(-)}|$ would be always smaller than $|\lambda_1^{(+)}/\lambda_0^{(+)}|$. Especially, the ratio $|\lambda_1^{(-)}/\lambda_0^{(-)}|$ approaches zero when $\cos \kappa$ is close to t_1/t_2 , which significantly accelerates the convergence of $\lambda^{(-)}(n)$ and exhibits typical ISSE [Fig. 3 (b)]. As κ approaches $\pm\pi/2$, the ratio $|\lambda_1^{(\pm)}/\lambda_0^{(\pm)}|$ diverges to infinity, which leads the ISSE becomes less apparent [Fig. 3 (c)].

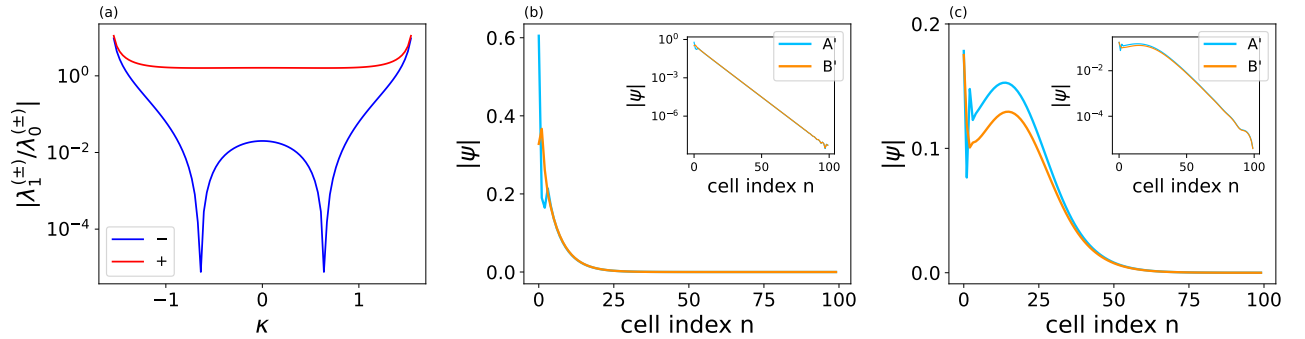


FIG. 3. (a) $|\lambda_1^{(\pm)}/\lambda_0^{(\pm)}|$ as a function of κ , for $\lim_{n \rightarrow \infty} (\gamma_n - \gamma_{n-1}) = 0$ (Eq. (23)). κ is ranging from $-\pi/2$ to $\pi/2$. (b), (c) The profile of eigenstate, the inset is eigenstate in log scale. $\gamma_n = 20 \ln(1 + n/100)$. For (b), energy $E = -0.270 - 0.079i$ ($\kappa = -0.560 - 0.185i$). For (c), energy $E = -0.485 - 0.025i$ ($\kappa = -1.272 - 0.168i$). For (a)-(c), $t_1 = 0.4$, $t_2 = 0.5$.

(2.) $\lim_{n \rightarrow \infty} (\gamma_n - \gamma_{n-1}) = \gamma_0$, where γ_0 is a constant. For example, linear function $\gamma_n = \gamma_0 n$.

In this type of γ_n function, both the $\frac{1}{\gamma_n}$ and $\frac{\gamma_n - \gamma_{n-1}}{\gamma_n}$ terms exhibit leading nontrivial contributions. Thus, the leading terms of $b(n)$, $c(n)$ and $\lambda^{(\pm)}(n)$ are

$$\begin{aligned} b(n) &= b_0 + \frac{b_1}{\gamma_n} + \dots \quad \text{where } b_1 = \frac{1}{t_2} [(t_1 + iE)\gamma_0 + 2(t_1^2 + t_2^2 - E^2 + 2iEt_1)], \\ c(n) &= c_0 + \frac{c_1}{\gamma_n} + \dots \quad \text{where } c_1 = 4t_1 + \gamma_0, \\ \lambda^{(\pm)}(n) &= \lambda_0^{(\pm)} + \frac{\lambda_1^{(\pm)}}{\gamma_n} + \dots \end{aligned} \quad (24)$$

Since the form of $b(n)$, $c(n)$ and $\lambda^{(\pm)}(n)$ are identical to those in (1.), $\lambda_1^{(\pm)}/\lambda_0^{(\pm)}$ can be derived using the same method, resulting in

$$\frac{\lambda_1^{(\pm)}}{\lambda_0^{(\pm)}} = \mp \frac{(t_1 \pm t_2 \cos \kappa)(t_1 \pm t_2 \cos \kappa + \gamma_0/2)}{t_2 \cos \kappa}. \quad (25)$$

The magnitude of the ratio, $|\lambda_1^{(-)}/\lambda_0^{(-)}|$, is generally smaller than that of $|\lambda_1^{(+)}/\lambda_0^{(+)}|$. Notably, as $\cos \kappa$ approaches either t_1/t_2 or $(t_1 + \gamma_0/2)/t_2$, the value of $|\lambda_1^{(-)}/\lambda_0^{(-)}|$ tends to zero.

(3.) $\lim_{n \rightarrow \infty} (\gamma_n - \gamma_{n-1}) = \infty$, but $\lim_{n \rightarrow \infty} \frac{\gamma_n - \gamma_{n-1}}{\gamma_n} = 0$. For example, polynomial function with degree larger than 1, $\gamma_n \sim n^\alpha$, where $\alpha > 1$.

The leading nontrivial term is $\frac{\gamma_n - \gamma_{n-1}}{\gamma_n}$ in this case. Expand $b(n)$, $c(n)$ and $\lambda^{(\pm)}(n)$ to the first-order approximation, we obtain

$$\begin{aligned} b(n) &= b_0 + b_1 \frac{\gamma_n - \gamma_{n-1}}{\gamma_n} + \dots \quad \text{where } b_1 = \frac{t_1 + iE}{t_2}, \\ c(n) &= c_0 + c_1 \frac{\gamma_n - \gamma_{n-1}}{\gamma_n} + \dots \quad \text{where } c_1 = 1, \\ \lambda^{(\pm)}(n) &= \lambda_0^{(\pm)} + \lambda_1^{(\pm)} \frac{\gamma_n - \gamma_{n-1}}{\gamma_n} + \dots \end{aligned} \quad (26)$$

Using the same method as in (1.), we can solve out $\lambda_1^{(\pm)}/\lambda_0^{(\pm)}$, and the result is

$$\frac{\lambda_1^{(\pm)}}{\lambda_0^{(\pm)}} = \mp \frac{t_1 \pm t_2 \cos \kappa}{t_2 \cos \kappa}. \quad (27)$$

Similar to (1.), the magnitude of the ratio $|\lambda_1^{(-)}/\lambda_0^{(-)}|$ would be always smaller than $|\lambda_1^{(+)}/\lambda_0^{(+)}|$. Besides, this ratio converges to zero as $\cos \kappa$ approaches t_1/t_2 .

(4.) $\lim_{n \rightarrow \infty} (\gamma_n - \gamma_{n-1}) = \infty$, and $\lim_{n \rightarrow \infty} \frac{\gamma_n - \gamma_{n-1}}{\gamma_n} = \text{constant}$. For example, exponential function $\gamma_n \sim e^{\alpha n}$.

In this case, the $\frac{\gamma_n - \gamma_{n-1}}{\gamma_n}$ term degenerates to constant. Therefore, the leading nontrivial term is the $\frac{1}{\gamma_n}$ term. The coefficients $b(n)$ and $c(n)$ can be expanded as Eq. (19) in (1.) with the same b_1 and c_1 , but b_0 and c_0 would have a shift due to degenerated $\frac{\gamma_n - \gamma_{n-1}}{\gamma_n}$ term. This effect only causes a shift in the value of $\lambda_0^{(\pm)}$ but maintains the convergence property of $\lambda^{(\pm)}(n)$.

V. THE RECURRENCE RELATION OF $\psi_n^{(\pm)}$ AND ITS APPROXIMATION

In this section, we derive the recurrence relation for $\psi_n^{(\pm)}$ and discuss the approximation used in the main article.

We decompose $|\psi(n)\rangle$ to the eigenvectors of $T(n)$, using $\psi_n^{(\pm)} = \langle \lambda_L^{(\pm)}(n) | \psi(n) \rangle$ to denote the $\langle \lambda_L^{(\pm)}(n) |$ component of $|\psi(n)\rangle$,

$$|\psi(n)\rangle = \sum_{i \in \{+, -\}} \psi_n^{(i)} |\lambda_R^{(i)}(n)\rangle. \quad (28)$$

Substituting Eq. (28) into Eq. (3), we get the recurrence relation between $\psi_{n-1}^{(\pm)}$ and $\psi_n^{(\pm)}$,

$$\psi_n^{(\pm)} = \lambda^{(\pm)}(n) \left[\langle \lambda_L^{(\pm)}(n) | \lambda_R^{(\pm)}(n-1) \rangle \psi_{n-1}^{(\pm)} + \langle \lambda_L^{(\pm)}(n) | \lambda_R^{(\mp)}(n-1) \rangle \psi_{n-1}^{(\mp)} \right]. \quad (29)$$

If γ_n is uniform, i.e. the system has discrete translational symmetry, the recurrence relation Eq. (29) simplifies to $\psi_n^{(\pm)} = \lambda^{(\pm)} \psi_{n-1}^{(\pm)}$. This is straightforward—the $\langle \lambda_L^{(\pm)}(n) |$ component is scaled by the corresponding eigenvalue $\lambda^{(\pm)}$. However, for general situations, We can see that $\psi_n^{(\pm)} \neq \lambda^{(\pm)}(n) \psi_{n-1}^{(\pm)}$, which means that if $|\psi(n-1)\rangle$ only have $|\lambda_R^{(+)}(n-1)\rangle$ part, $|\psi(n)\rangle$ will have both $|\lambda_R^{(+)}(n)\rangle$ part and $|\lambda_R^{(-)}(n)\rangle$ part. This is because transfer matrix $T(n-1)$ differs from $T(n)$, introducing a mixed term $\langle \lambda_L^{(\pm)}(n) | \lambda_R^{(\mp)}(n-1) \rangle \psi_{n-1}^{(\mp)}$. However, if we assume that transfer matrix $T(n)$ varies slowly, then $\langle \lambda_L^{(\pm)}(n) | \lambda_R^{(\pm)}(n-1) \rangle \approx 1$ and $\langle \lambda_L^{(\pm)}(n) | \lambda_R^{(\mp)}(n-1) \rangle \approx 0$. Consequently, the recurrence relation Eq. (29) can be approximated as follows:

$$\psi_n^{(\pm)} \approx \lambda^{(\pm)}(n) \psi_{n-1}^{(\pm)}, \quad (30)$$

unless $|\psi_n^{(\mp)}| \gg |\psi_n^{(\pm)}|$.

VI. ANALYSIS OF PARAMETERS

In this section, we discuss the impact of parameters, including hopping parameters t_1, t_2 and chain length L , on the ISSE in our model.

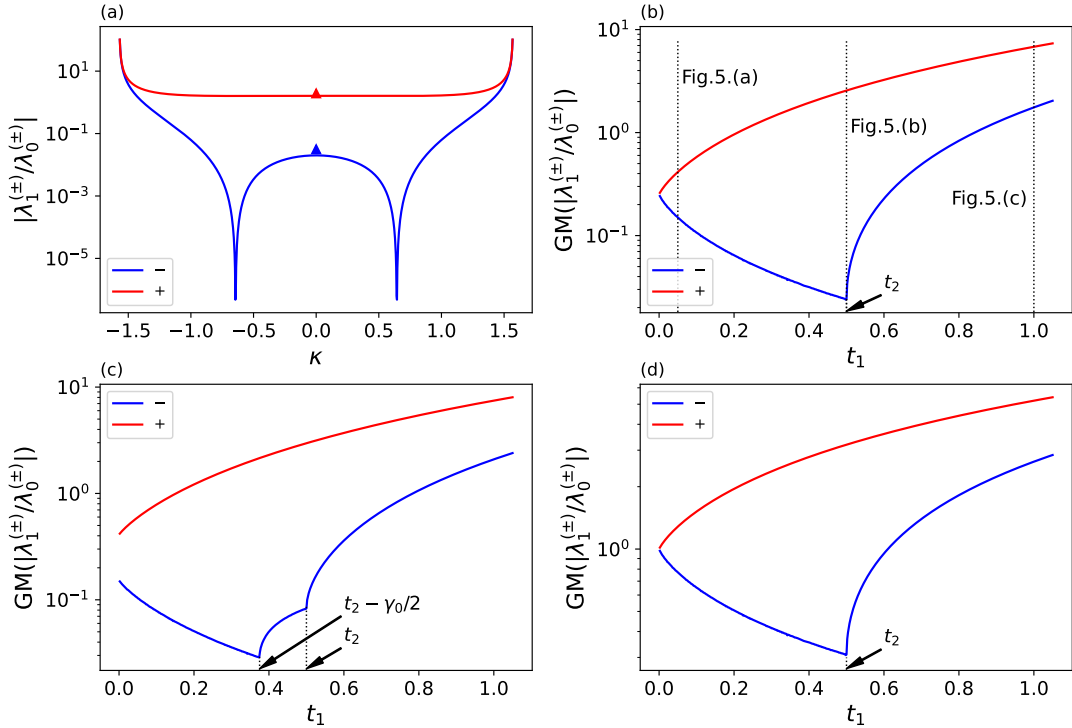


FIG. 4. (a) $|\lambda_1^{(\pm)}/\lambda_0^{(\pm)}|$ as a function of κ when t_1 and t_2 fixed. κ is ranging from $-\pi/2$ to $\pi/2$. The triangle is geometric mean of $|\lambda_1^{(\pm)}/\lambda_0^{(\pm)}|$. parameters are $t_1 = 0.4$, $t_2 = 0.5$ and $\gamma_n = 0.25n$. (b), (c), (d) Geometric mean of $|\lambda_1^{(\pm)}/\lambda_0^{(\pm)}|$ as a function of t_1 . $t_2 = 0.5$. $\lim_{n \rightarrow \infty} (\gamma_n - \gamma_{n-1}) = 0$ for (b). $\lim_{n \rightarrow \infty} (\gamma_n - \gamma_{n-1}) = \gamma_0 = 0.25$ for (c). $\lim_{n \rightarrow \infty} (\gamma_n - \gamma_{n-1}) = \infty$, but $\lim_{n \rightarrow \infty} \frac{\gamma_n - \gamma_{n-1}}{\gamma_n} = 0$ for (d). Three vertical dotted lines in (b) indicates the parameters of Fig.5.

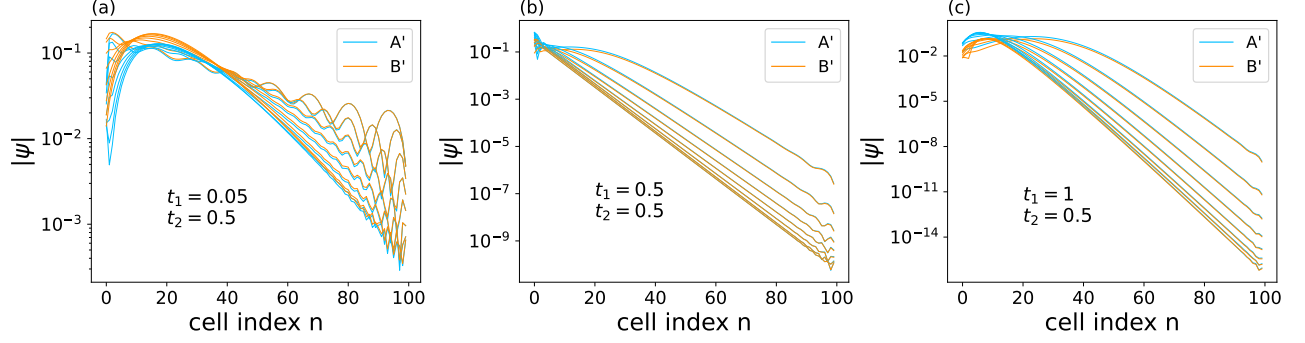


FIG. 5. Profile of eight randomly chosen eigenstates from ‘-’ part of spectrum. The parameters are $t_2 = 0.5$, $\gamma_n = 20 \ln(1 + n/100)$. $t_1 = 0.05$ for (a), $t_1 = 0.5$ for (b), $t_1 = 1$ for (c). These parameter selections correspond to the illustration provided in Fig.4(b).

A. t_1 and t_2

In the main article, we state that in order to generate evident ISSE, the $\lambda^{(-)}(n)$ should converge to $\lambda_0^{(-)}$ quickly and converges much faster than $\lambda^{(+)}(n)$, namely

$$\left| \lambda_1^{(-)} / \lambda_0^{(-)} \right| \ll 1, \quad \left| \lambda_1^{(-)} / \lambda_0^{(-)} \right| \ll \left| \lambda_1^{(+)} / \lambda_0^{(+)} \right|. \quad (31)$$

Subsequently, we investigate how the model parameters, t_1 and t_2 , impact $\lambda_1^{(\pm)} / \lambda_0^{(\pm)}$ to satisfy this condition.

In Sec. IV of the supplemental material, we show that $\lambda_1^{(\pm)} / \lambda_0^{(\pm)}$ are determined by the parameters t_1 , t_2 and κ . And we have argued that in thermodynamic limit the parameter κ can be effectively approximated by the corresponding k in A-B decoupled case, which ranges from $-\pi/2$ to $\pi/2$. To characterise the convergence speed of $\lambda^{(\pm)}$ under fixed parameters t_1 and t_2 , while excluding the influence of κ , we concentrate on the geometric mean [4] of $|\lambda_1^{(\pm)} / \lambda_0^{(\pm)}|$ across κ as a metric [Fig. 4(a)]. This choice is made because the arithmetic mean of $|\lambda_1^{(\pm)} / \lambda_0^{(\pm)}|$ across κ diverges in this context. The geometric mean is given by

$$GM \left(\left| \frac{\lambda_1^{(\pm)}}{\lambda_0^{(\pm)}} \right| \right) = \text{Exp} \left[\frac{1}{\pi} \int_{-\pi/2}^{\pi/2} \ln \left(\left| \frac{\lambda_1^{(\pm)}}{\lambda_0^{(\pm)}} \right| \right) d\kappa \right]. \quad (32)$$

We can depict $GM(|\lambda_1^{(\pm)} / \lambda_0^{(\pm)}|)$ as a function of t_1 for fixed t_2 [Fig. 4(b), (c), (d)].

As an example, we focus on the $\lim_{n \rightarrow \infty} (\gamma_n - \gamma_{n-1}) = 0$ case [Fig. 4(b)]. A similarity can be shown for other types of γ_n function. Recall the convergence speed Eq. (23),

$$\frac{\lambda_1^{(\pm)}}{\lambda_0^{(\pm)}}(\kappa) = \mp \frac{(t_1 \pm t_2 \cos \kappa)^2}{t_2 \cos \kappa}. \quad (33)$$

The critical point of Eq. (33) is $t_1 = t_2$, since a real zero point $\kappa = \arccos(t_1/t_2)$ exists when $t_1 \leq t_2$. It's plain that $GM(|\lambda_1^{(+)} / \lambda_0^{(+)}|)$ increases with t_1 . For $GM(|\lambda_1^{(-)} / \lambda_0^{(-)}|)$, it decreases as t_1 increases from 0, attains minimum at critical point $t_1 = t_2$, and then increases with t_1 . Therefore, when t_1 is in proximity to t_2 , the condition stated in Eq. (31) can be effectively met, leading to a typical ISSE behavior [Fig.5(b)]. However, if t_1 is significantly smaller or larger than t_2 , the features of ISSE would weaken, manifesting as an initial increase followed by a decrease in the wave function from left to right, resulting in a peak formation near the left boundary [Fig.5(a), (c)].

B. Chain Length L

In the preceding section of this paper, we analyze the model in thermodynamic limit, where the loss rate γ_n exhibits monotonic growth, ultimately diverging to positive infinity as $n \rightarrow \infty$. However, based on the analysis of the reason for ISSE in our model, as long as the loss rate in the lattice is increased to a sufficiently large value such that $\lambda^{(-)}(n)$

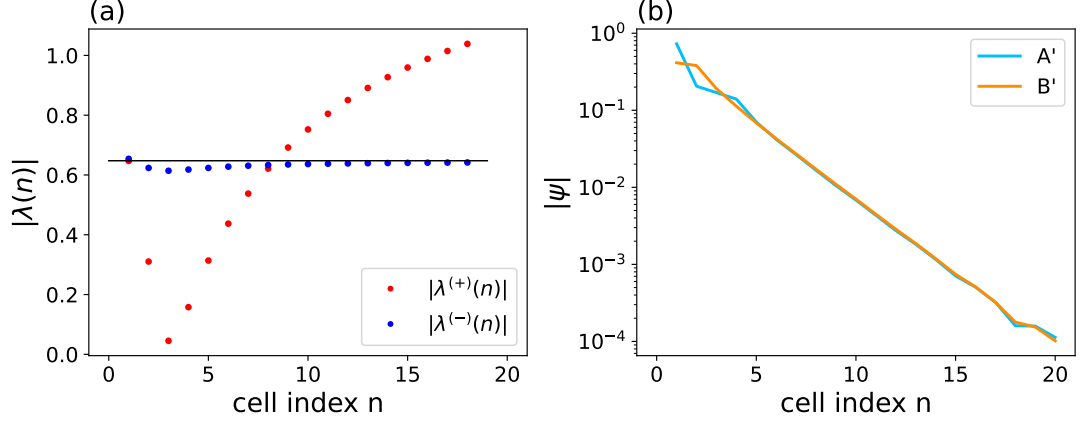


FIG. 6. (a) The modulus of $|\lambda^{(\pm)}(n)|$ and (b) the profile of eigenstate $|\psi|$ as function of cell index n , for an eigenstate whose $|\lambda_1^{(-)}/\lambda_0^{(-)}| \approx 3.78 \times 10^{-2}$ in a short lattice with length $L = 20$. The parameters are $t_1 = 0.4$, $t_2 = 0.5$ and $\gamma_n = 0.25n$, and the energy of the eigenstate is $E \approx -0.291 - 0.190i$. The horizontal black lines in (a) is $\lambda_0^{(-)}$.

can converge to $\lambda_0^{(-)}$, i.e. $\left|(\lambda^{(-)}(L) - \lambda_0^{(-)})/\lambda_0^{(-)}\right| \ll 1$, where L is the length of lattice, then an apparent ISSE will appear. So it's possible to exhibit this effect in a short lattice, which provides the feasibility of future experimental investigation with finite-size systems on this model. [Fig. 6] shows a numerical example with linearly increasing loss rate in a short lattice. In this example, the length of lattice L is only 20 and $\gamma_L = 5$, which is far from 'infinity', but it's enough for $\lambda^{(-)}(n)$ to converge to $\lambda_0^{(-)}$ [Fig. 6(a)],

$$\left|\frac{\lambda^{(-)}(L) - \lambda_0^{(-)}}{\lambda_0^{(-)}}\right| \approx \left|\frac{\lambda_1^{(-)}}{\lambda_0^{(-)}} \frac{1}{\gamma_L}\right| \approx 7.2 \times 10^{-3} \ll 1. \quad (34)$$

So it presents the apparent ISSE with uniform decay rate and non-interference [Fig. 6(b)].

-
- [1] The convergence of eigenvalue perturbation series is a subtle problem in quantum mechanics, with many well-known cases exhibiting divergence. Nevertheless, our focus here is on a system with a finite chain length L , with a correspondingly finite dimension of its Hilbert space. This finite dimensionality ensures the convergence of perturbation theory in this specific scenario [?]. Subsequently, we delve into an analysis of how the perturbed eigenvalues evolve with increasing L .
 - [2] G. H. Wannier, Dynamics of band electrons in electric and magnetic fields, *Rev. Mod. Phys.* **34**, 645 (1962).
 - [3] T. Hartmann, F. Keck, H. Korsch, and S. Mossmann, Dynamics of bloch oscillations, *New Journal of Physics* **6**, 2 (2004).
 - [4] M. F. Triola, *Elementary Statistics Technology Update* (Addison Wesley Longman, 2012).